East Africa Rainfall Trends and Variability 1983-2015 Using Three Long-term Satellite Products

E. Cattani, A. Merino, J. A. Guijarro, and V. Levizzani

SUPPLEMENTARY MATERIAL

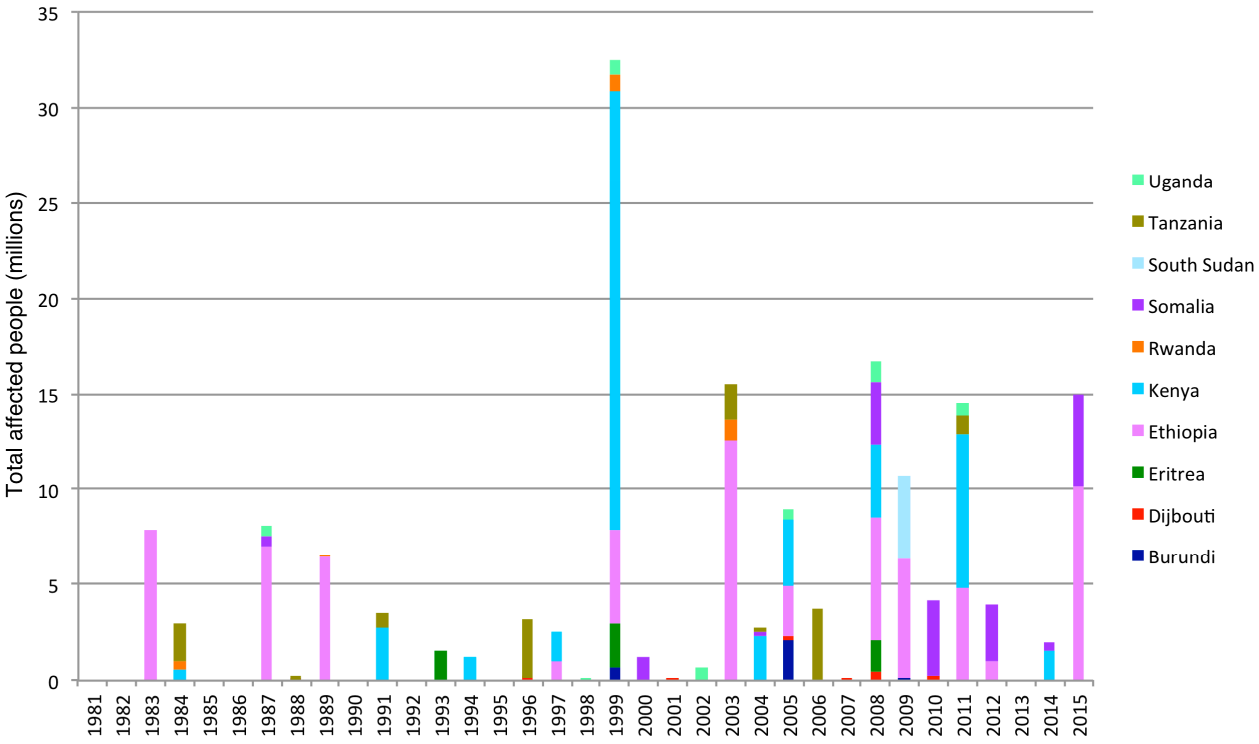

Figure S1. Total affected people during the drought events in EA from 1981. Total affected people include people requiring immediate assistance during the emergency period, i.e., basic survival needs such as food, water, shelter, sanitization, and immediate medical assistance. Data are courtesy of D. Guha-Sapir, R. Below, Ph. Hoyois, EM-DAT: Emergency Events Database, http://www.emdat.be, Université Catholique de Louvain, Brussels, Belgium.

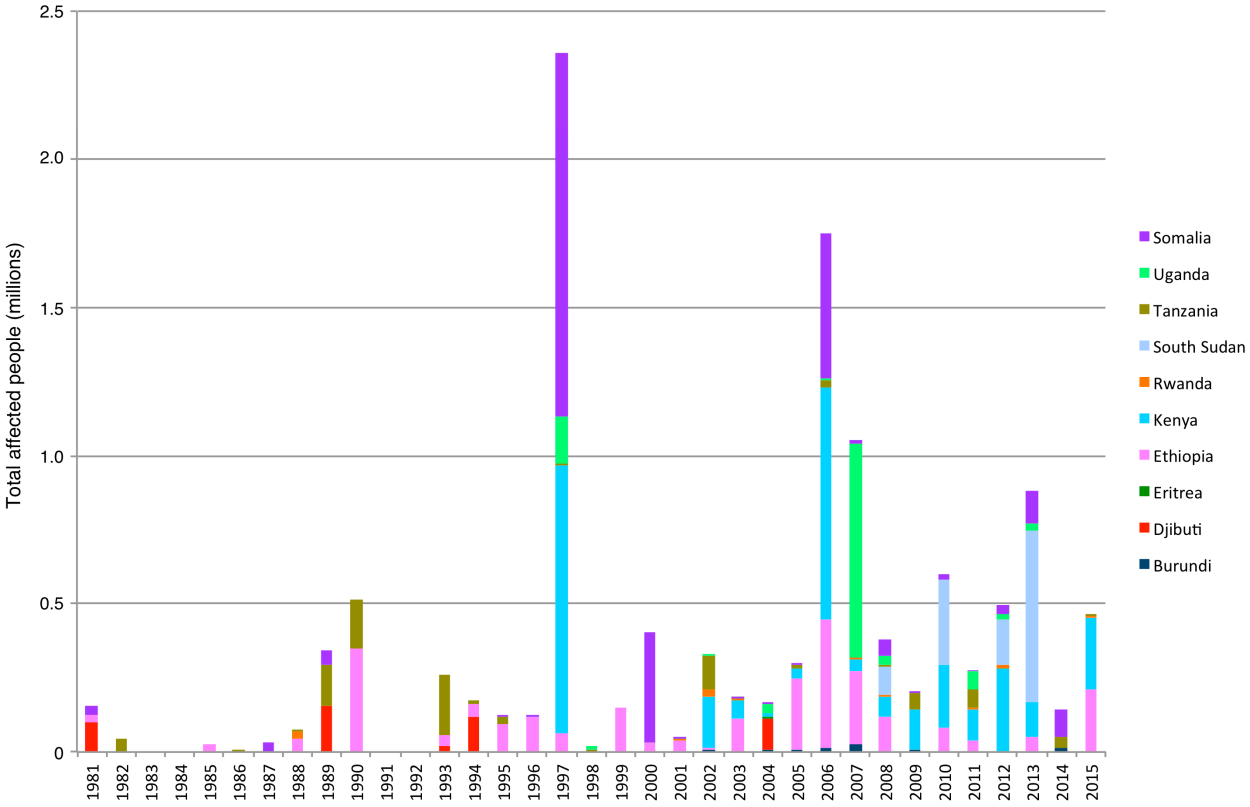

Figure S2. Same as in Figure S1 but for flood events.

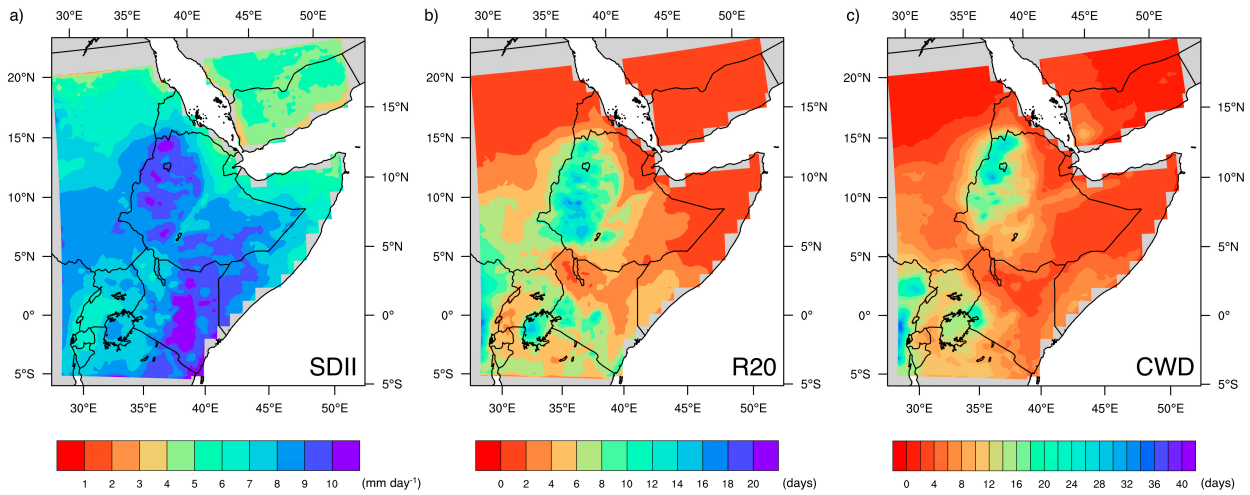

Figure S3. Maps of the annual climatology of SDII (a); R20 (b); CWD (c). For each annual index and satellite product the annual climatology was first computed, followed by the average over the three products (ensemble mean).

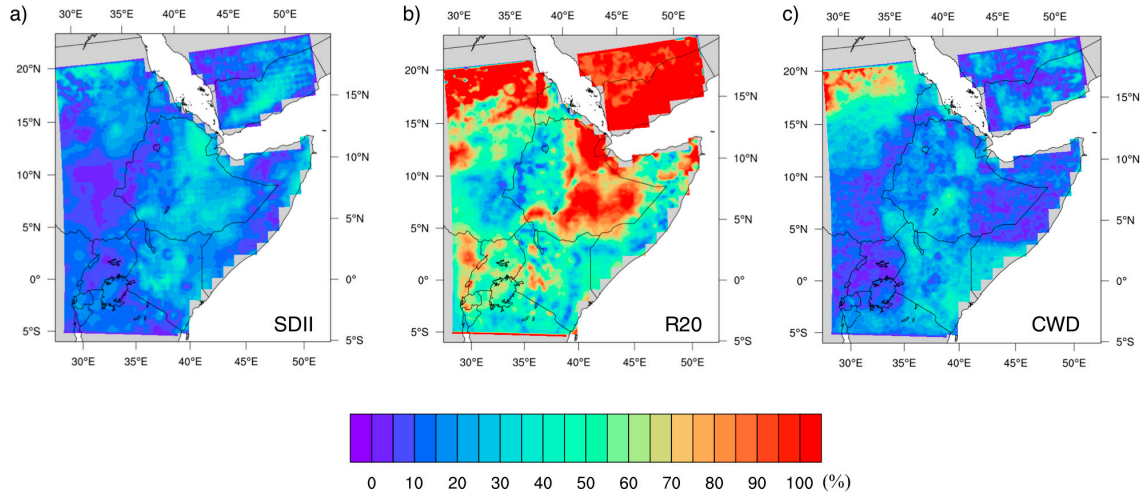

Figure S4. Maps of ensemble mean standard deviations of the rainfall indices in Figure S3, expressed as percentage of the three products ensemble mean: SDII (**a**), R20 (**b**), and CWD (**c**).

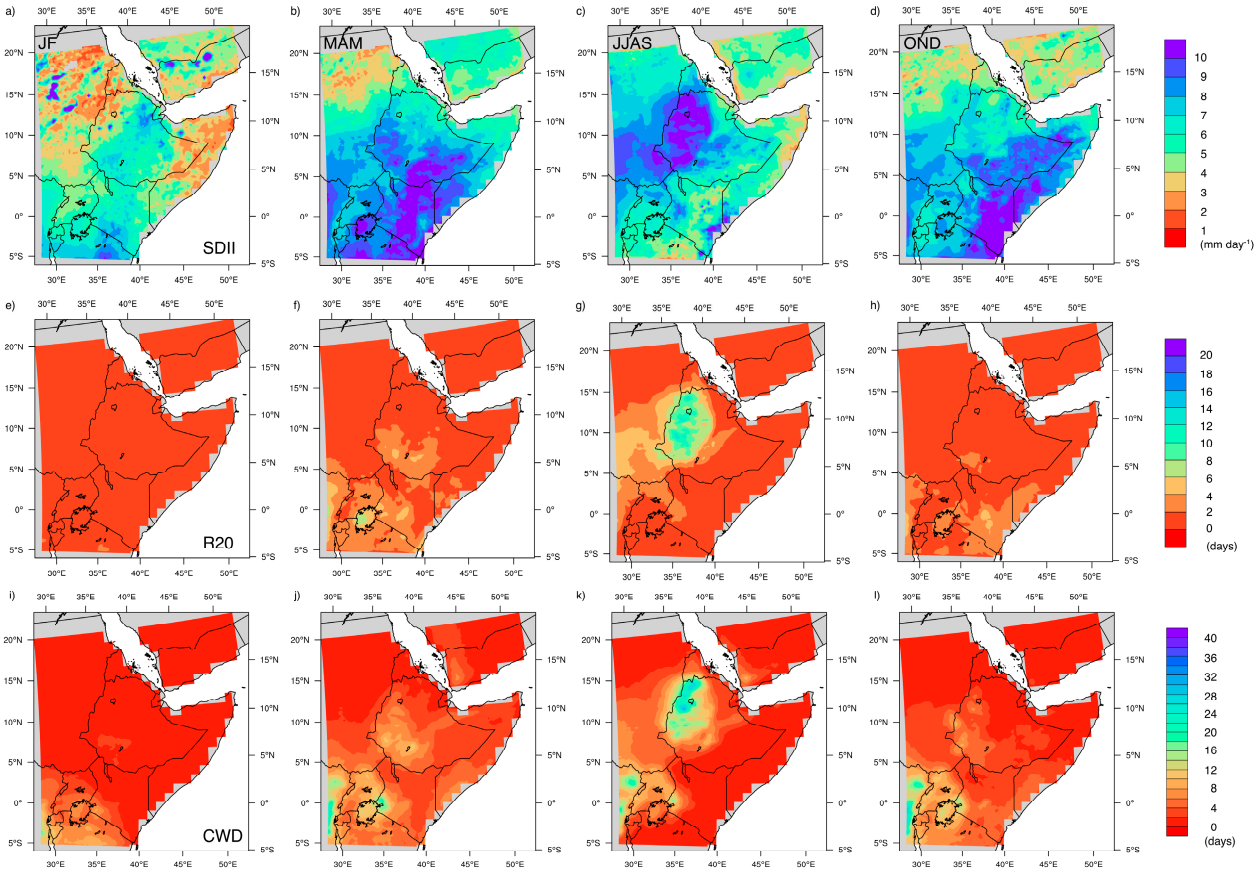

Figure S5 Maps of seasonal rainfall index climatology: SDII (a-d); R20(e-h); CWD (i-l). Each column of the plate refers to a season in the following order, January–February (JF), March–April–May (MAM), June–July–August–September (JJAS), and October–November–December (OND). Indices were computed with the same procedure of the annual indices but taking seasons as reference periods.

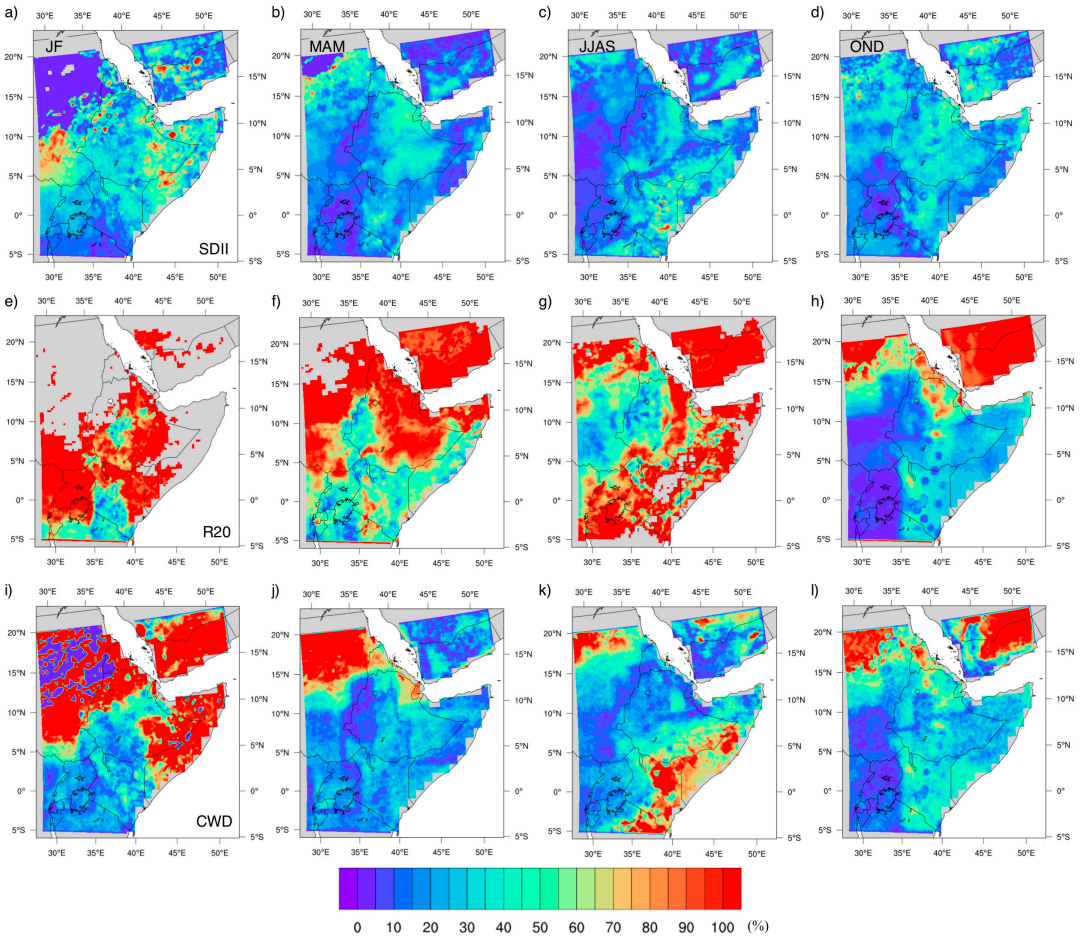

Figure S6. Maps of ensemble mean standard deviations of the seasonal rainfall indices in Figure S5, expressed as percentage of the three products' ensemble mean: SDII (**a**–**d**); R20(**e**–**h**); CWD (**i**–**l**).

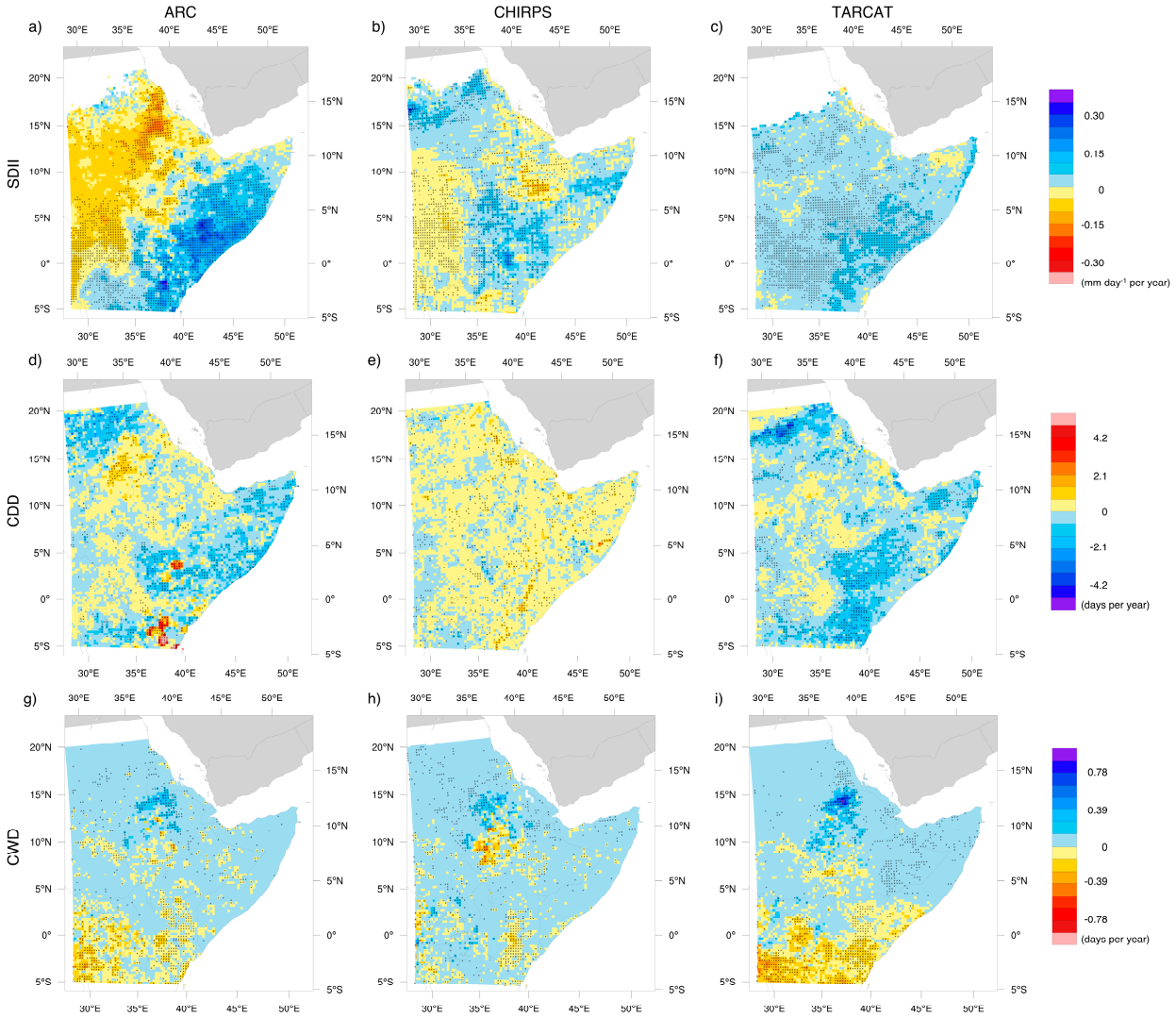

Figure S7. Sen slope estimator maps relative to annual trends of SDII (**a-c**), CDD (**d-f**), and CWD (**g-i**) for ARC (left column), CHIRPS (central column), and TARCAT (right column) data sets. Stippled grid cells display statistically significant trend at confidence levels ≥ 95%.

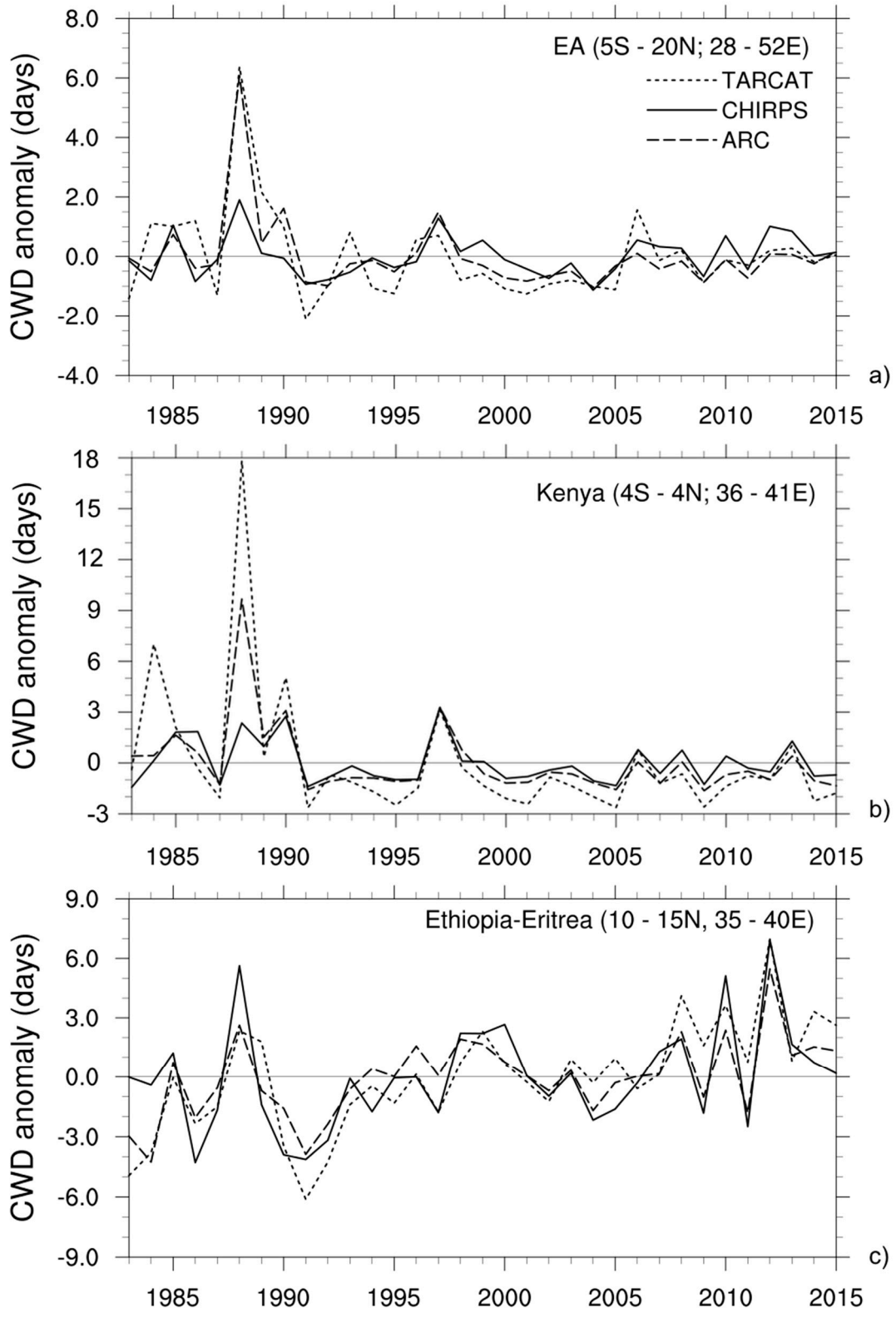

Figure S8. Annual CWD anomaly time series: ARC (long-dashed), TAMSAT (short-dashed), and CHIRPS (solid). Anomalies have been averaged over the whole EA (**a**), Kenya (**b**), Ethiopia-Eritrea (**c**).

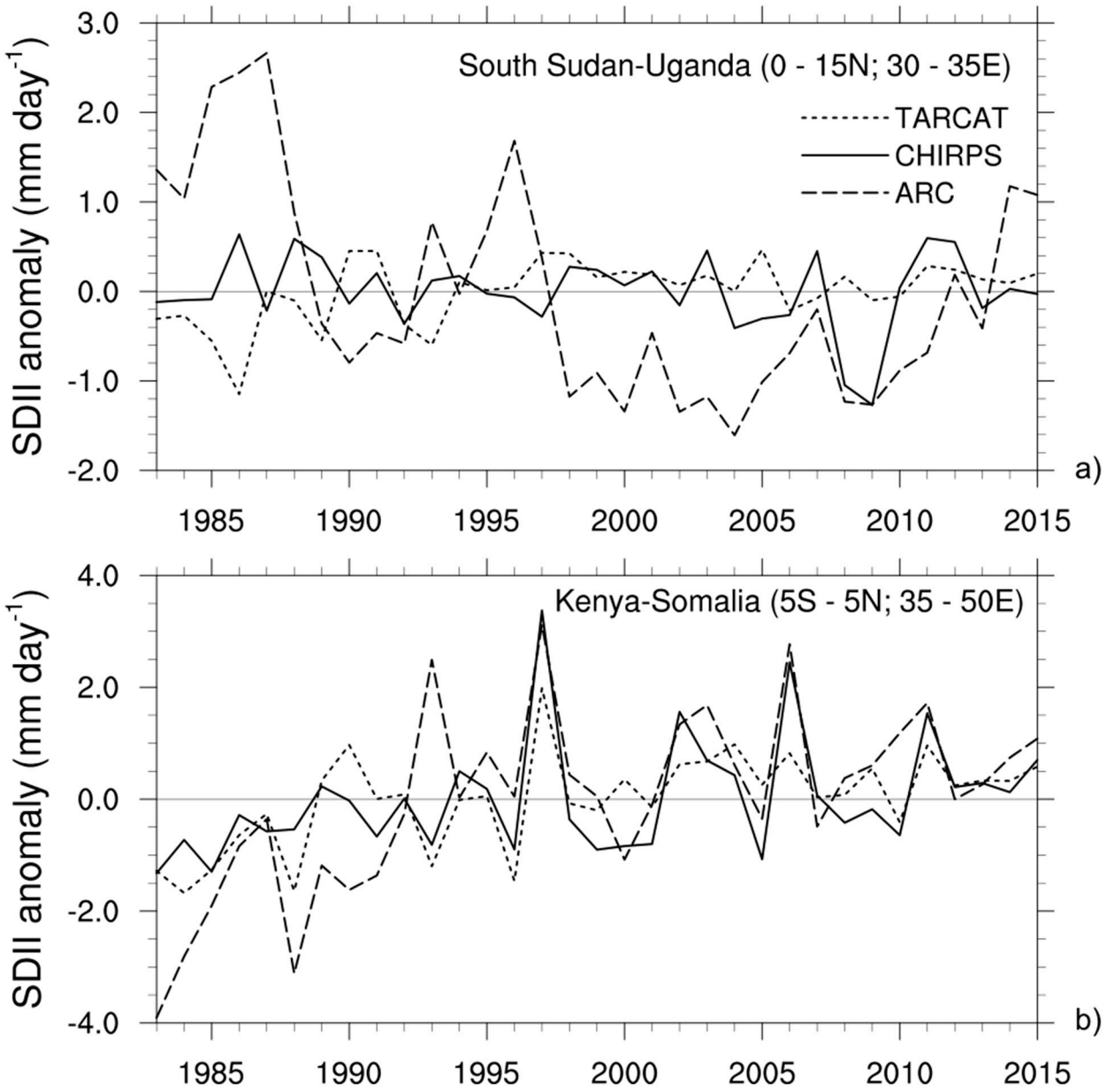

Figure S9. Annual SDII anomaly time series over South Sudan-Uganda (**a**) and Kenya-Somalia (**b**).

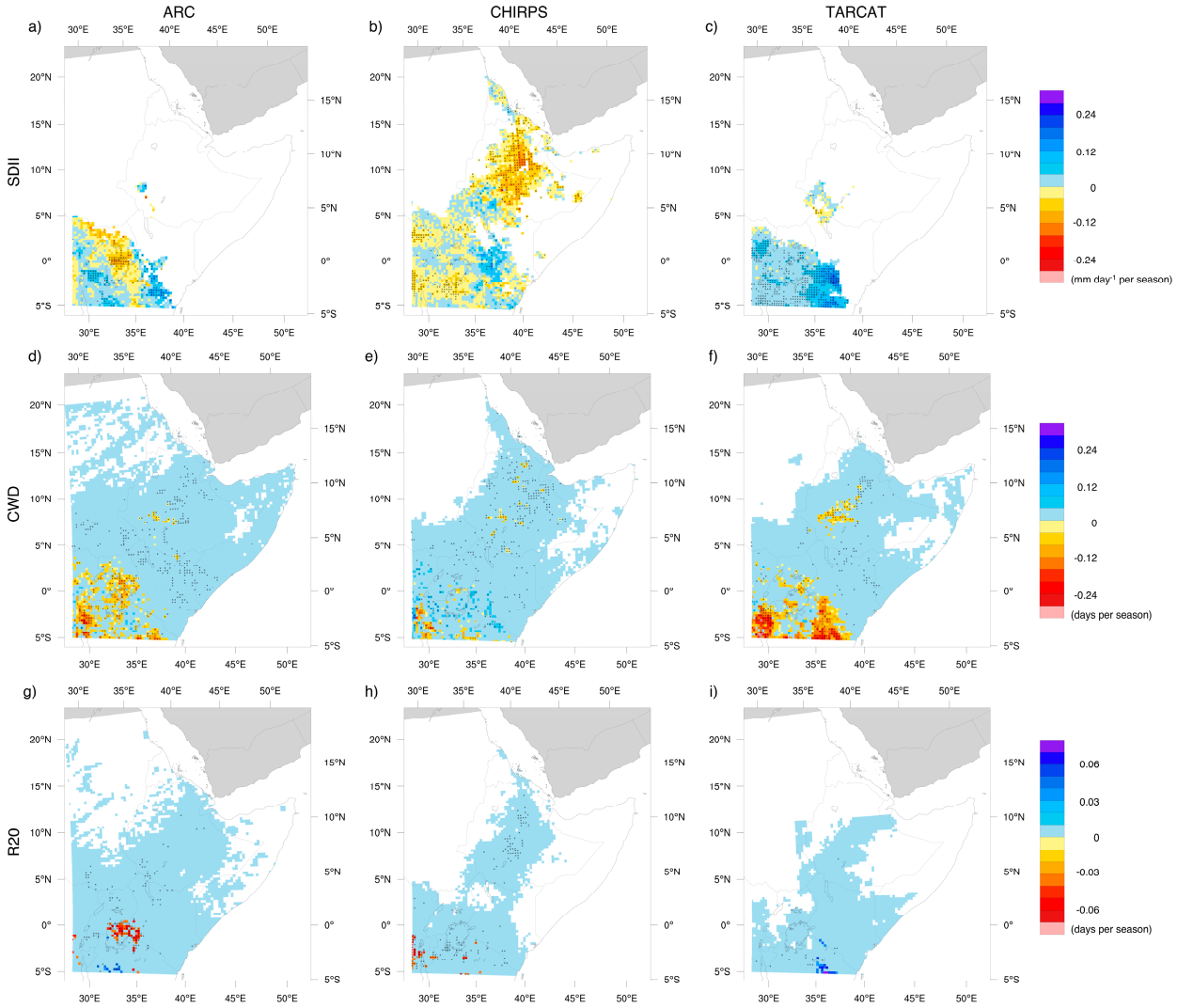

Figure S10. Same as in Figure S7, but for JF SDII (**a-c**), CWD (**d-f**), and R20 (**g-i**).

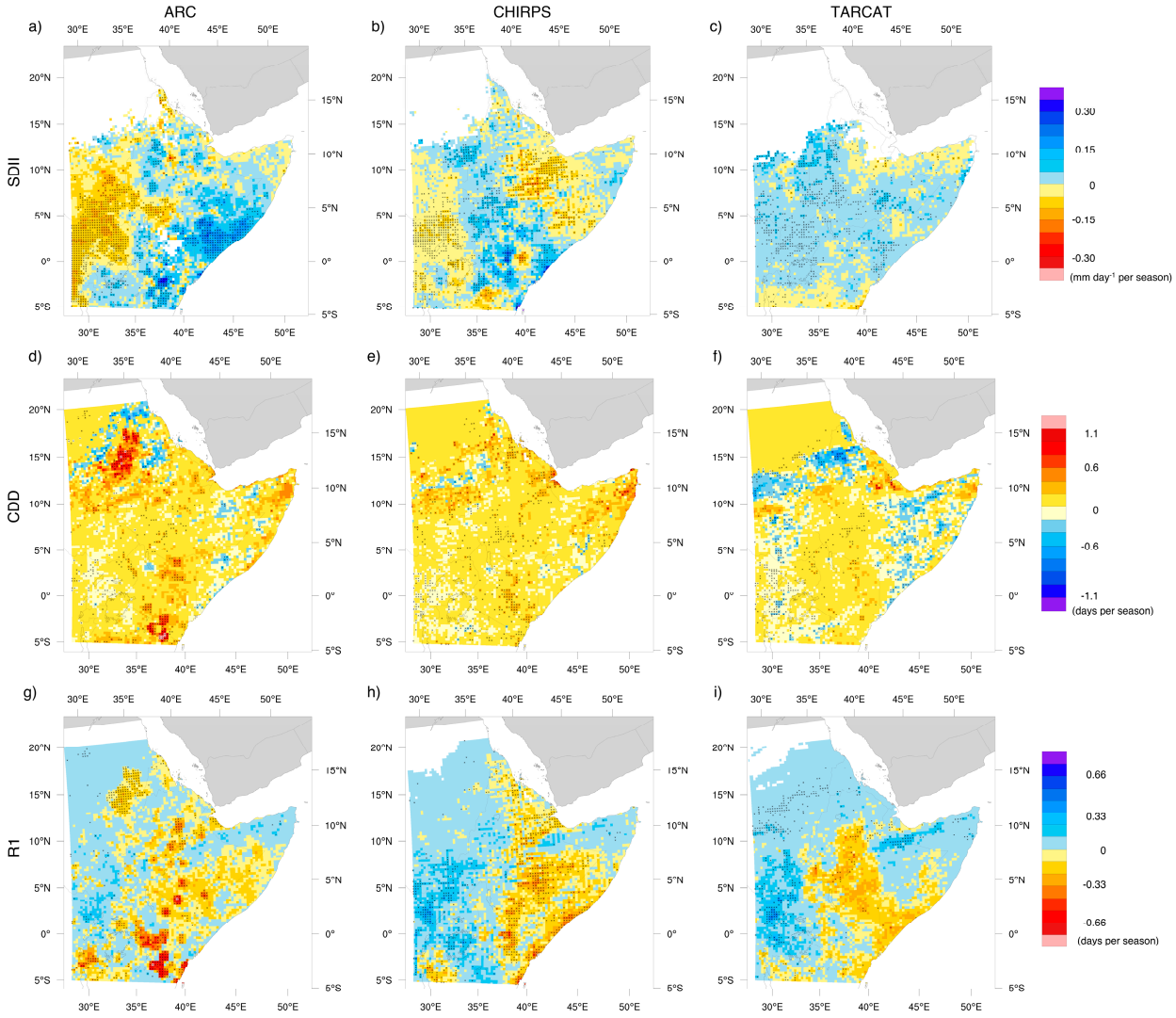

Figure S11. Same as in Figure S7, but for MAM SDII (**a-c**), CDD (**d-f**), and R1 (**g-i**).

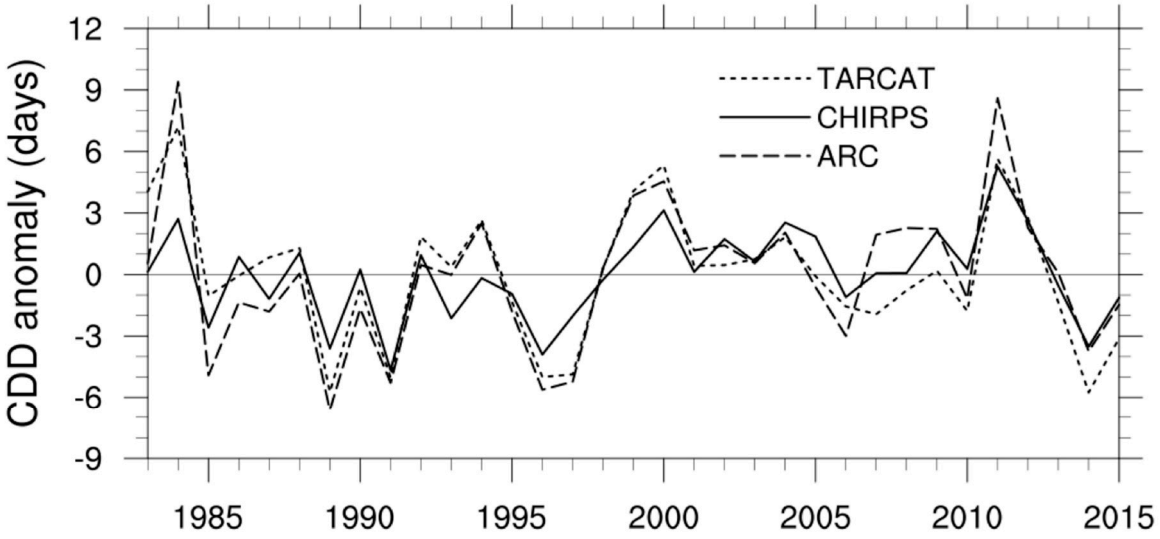

Figure S12. MAM CDD anomaly time series over the whole EA.

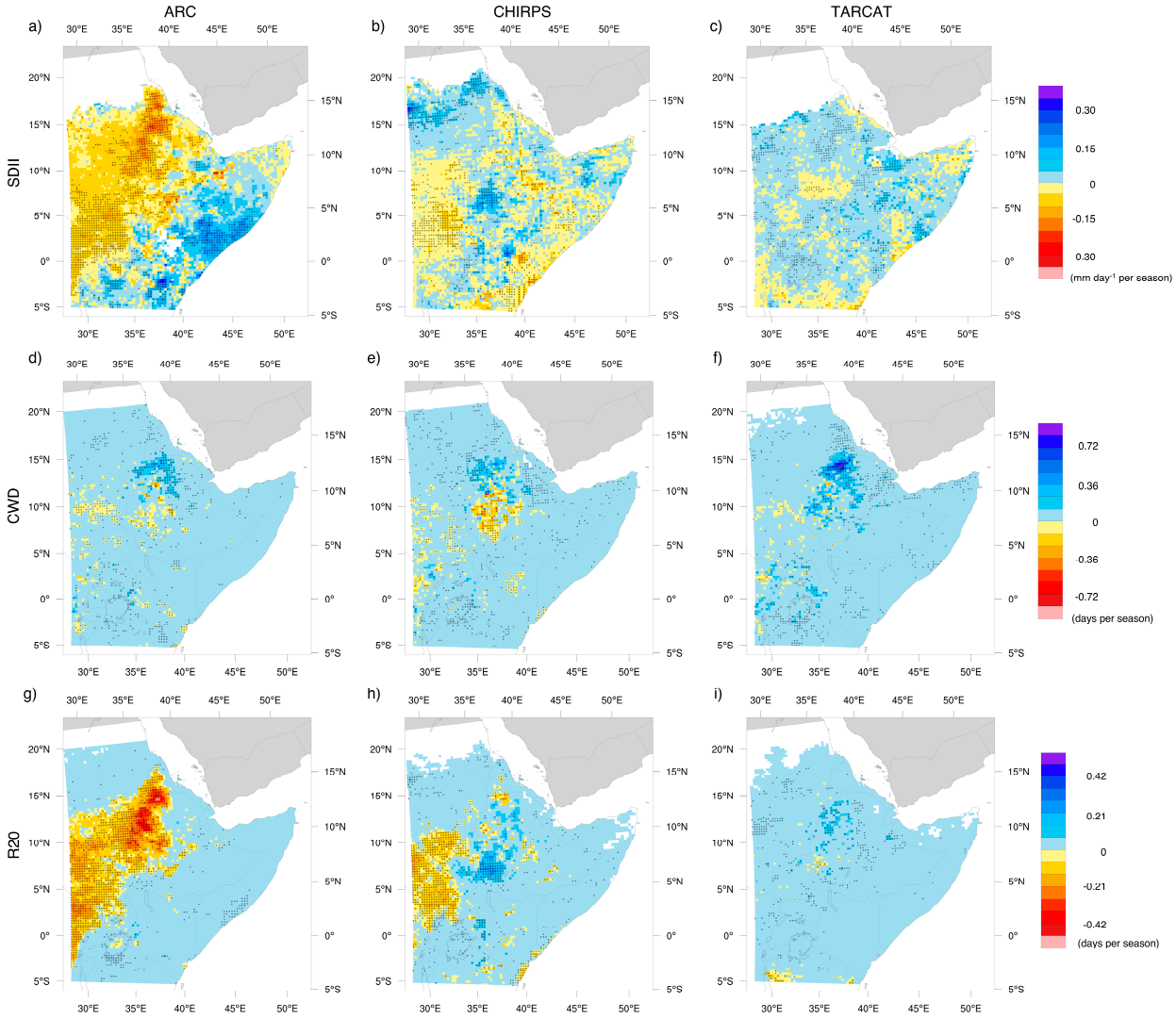

Figure S13. Same as in Figure S7, but for JJAS SDII (**a-c**), CWD (**d-f**), and R20 (**g-i**).

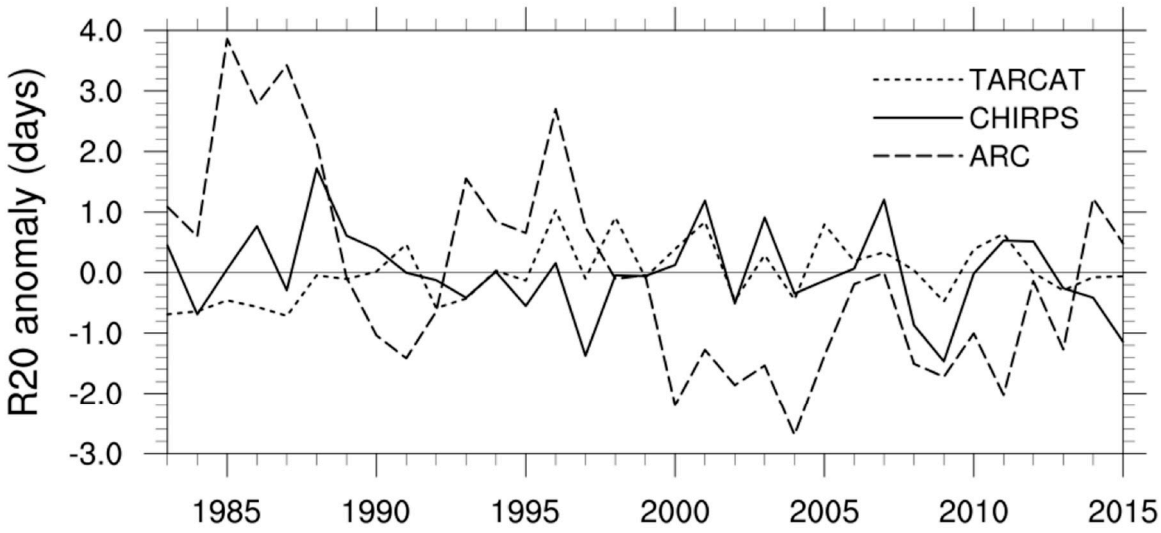

Figure S14. JJAS R20 anomaly time series over western EA.

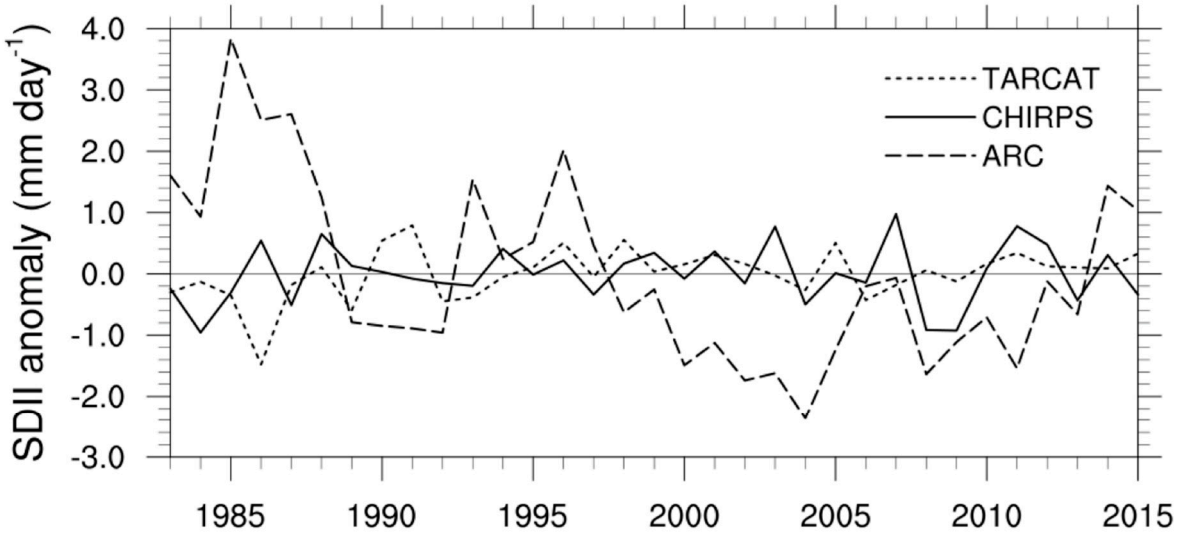

Figure S15. JJAS SDII anomaly time series over western EA.

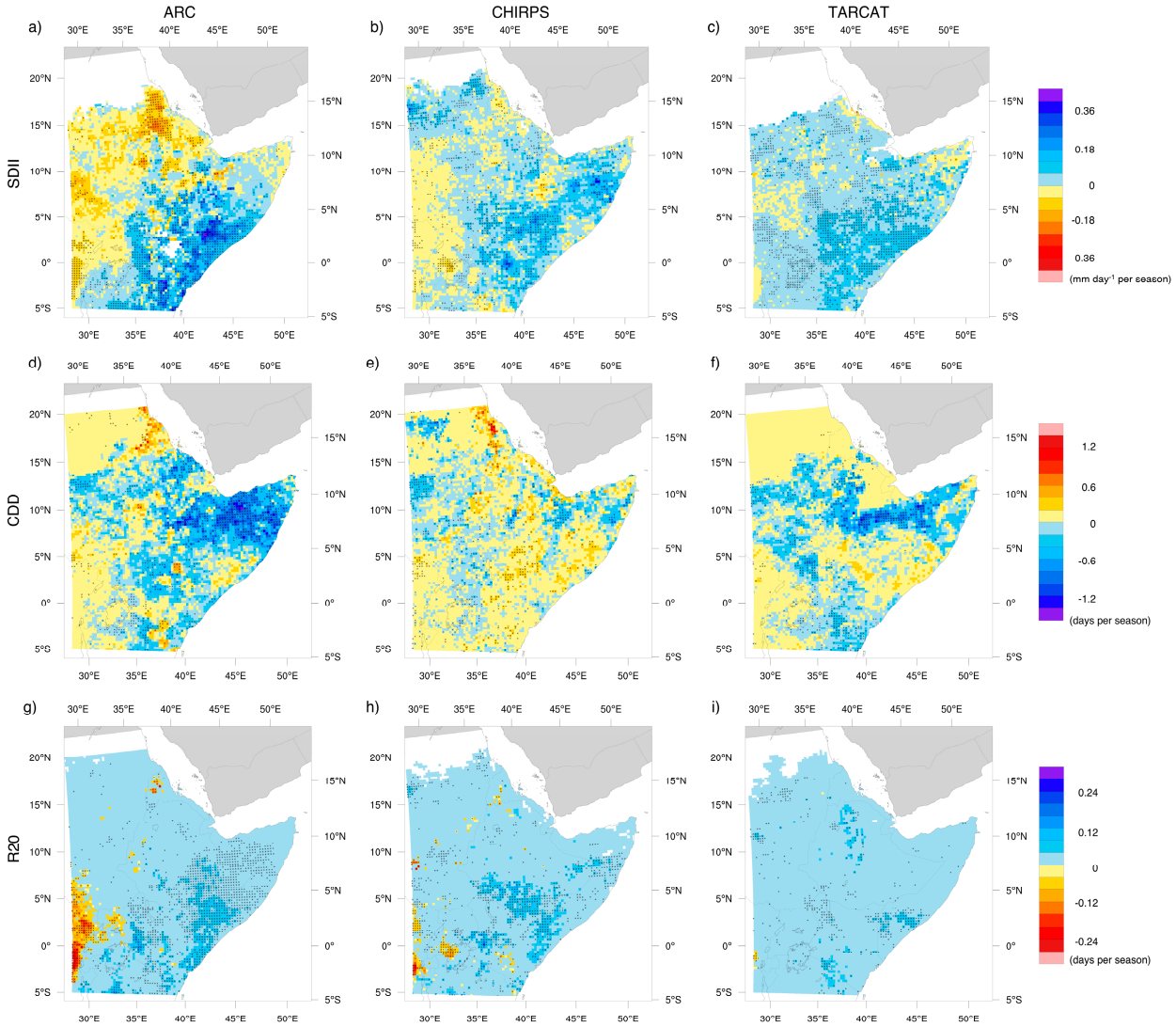

Figure S16. Same as in Figure S7, but for OND SDII (**a-c**), CDD (**d-f**), and R20 (**g-i**).

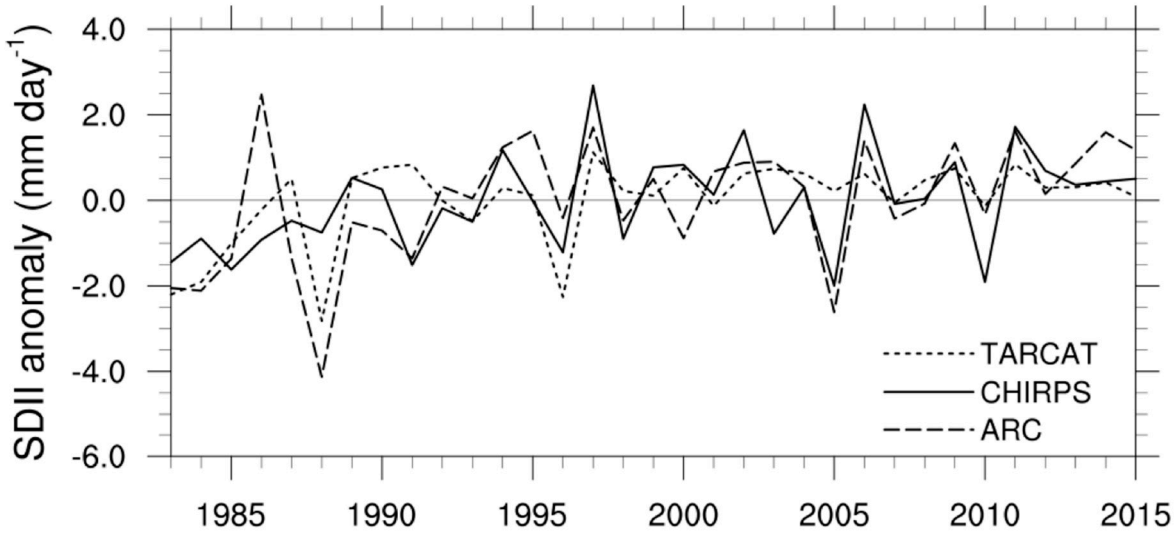

Figure S17. OND SDII anomaly time series over eastern EA.